12,05

Magnetic structure of $Co_{0.8-x}Mn_xZn_{0.2}Fe_2O_4$ nanoparticles ($x = 0.6$, 0.4 and 0.2) promising for biomedical applications

© A.S. Kamzin[1], V.G. Semenov[2], I.A. Al-Omari[3], V. Narayanaswamy[4], B. Issa[4,5,6]

[1] Ioffe Institute,
St. Petersburg, Russia
[2] St. Petersburg State University,
St. Petersburg, Russia
[3] Department of Physics, Sultan Qaboos University,
P.O. Box 36, Muscat PC 123, Sultanate of Oman
[4] Research Institute of Medical & Health Sciences, University of Sharjah,
Sharjah, P.O. Box 27272, United Arab Emirates
[5] Department of Medical Diagnostic Imaging, College of Health Sciences, University of Sharjah,
Sharjah P.O. Box 27272, United Arab Emirates
[6] Department of Biomedical Engineering, Faculty of Engineering and Natural Sciences, Istinye University,
Istanbul, 34010, Turkey

E-mail: ASKam@mail.ioffe.ru

Received June 25, 2023
Revised June 25, 2023
Accepted June 26, 2023

Magnetic nanoparticles (MNP) of ferrite $Co_{0.8-x}Mn_xZn_{0.2}Fe_2O_4$ ($x = 0.6$, 0.4 and 0.2) were synthesized by co-deposition. The structural, microstructural, magnetic and ultrathin properties of the obtained particles were investigated by X-ray diffraction and Mössbauer spectroscopy. The nanoparticle sizes calculated from radiographs at $x = 0.6$, 0.4 and 0.2 are 15.2, 10.2 and 10.3 nm, respectively. The influence of the amount of Mn ions introduced on the properties of synthesized particles has been studied. The analysis of experimental Mössbauer spectra showed that the small size of the MNP leads to a significant increase in the effects of dimensionality and the influence of the surface on the magnetic structure of the surface layer. The Mössbauer studies, for the first time without the use of external magnetic fields, on the example of MNP spinel ferrites $Co_{0.8-x}Mn_xZn_{0.2}Fe_2O_4$, found that inside the particle the magnetic moments are ordered collinearly, whereas in the surface layer the moments are oriented at an angle to each other (canting structure).

Keywords: spinel ferrites, Mössbauer spectroscopy, superparamagnetism, materials for biomedicine.

DOI: 10.61011/PSS.2023.08.56586.122

1. Introduction

Magnetic nanoparticles (MNP) of spinel ferrites are widely studied due to the huge potential of their applications. This is due to the unique properties of MNP spinel ferrites, their excellent magnetic characteristics, often accompanied by other useful functional properties, such as catalytic activity. The most important thing in magnetic MNP of spinel ferrites is the ability to control their magnetic properties to increase efficiency in a variety of applications, including biomedical ones, such as targeted drug delivery to the focus of the disease, increased contrast in MRT, magnetic hyperthermia, etc. [1–6]. In magnetic hyperthermia, MNP purposefully delivered to the area of a malignant tumor are used as generators of local heating to temperatures of $\sim 45^\circ$C. At this temperature, the death of malignant cells occurs, while healthy cells are not affected [3]. MNP should have certain properties for biomedical applications. So, the particle size for magnetic hyperthermia should be close to the superparamagnetic threshold, so that when 45°C is reached, the heating of particles by an external magnetic field is automatically turned off, because higher temperatures are dangerous for healthy cells [6]. A unique property of nanoparticles is the superparamagnetic state, which is absent in macroscopic crystals and consists in the destruction of the magnetic spin ordering by thermal fluctuations in the temperature range below the Curie temperature (T_C) [5].

Iron oxide (magnetite Fe_3O_4, maghemite g-Fe_2O_3) spinel ferrite (SF) MNP widely used in biomedicine currently do not meet the requirements of modern biomedicine due to their magnetic and other the properties and the task of the researchers was to create new MNP with the necessary parameters, while not inferior to iron oxides in biocompatibility. Numerous studies showed that SF particles of the type MFe_2O_4, where $M = Mg^{2+}$, Fe^{2+}, Co^{2+}, Ni^{2+}, Cu^{2+}, Zn^{2+} are such particles [4–6]. The unique properties of SF, such as high electrical resistivity and low eddy current losses, high saturation magnetization and T_C, mechanical hardness, high thermodynamic stability and corrosion resistance determine the wide application of SF in a wide variety of fields, including biomedicine.

$CoFe_2O_4$, $ZnFe_2O_4$ and $MnFe_2O_4$ ferrites having different structures, degrees of toxicity and a variety of applications attracted significant attention of researchers. Thus, magnetically hard cobalt ferrite ($CoFe_2O_4$) is an inverse structure in which divalent cations Co^{2+} occupy octahedral positions, and trivalent cations Fe^{3+} equally occupy tetrahedral and octahedral positions. Ferrite $CoFe_2O_4$ has a high coercive force, moderate saturation magnetization (80 emu/g at room temperature), high T_C — 520°C, large magnetocrystalline anisotropy, large magnetostrictive coefficient, chemical stability, mechanical hardness. All these properties of cobalt ferrite make it one of the promising materials for various applications, including biomedical [5–11]. Unlike cobalt ferrite, $MnFe_2O_4$ and $ZnFe_2O_4$ have a normal spinel structure in which divalent Zn^{2+}cations occupy tetrahedral positions, and trivalent cations Fe^{3+} — only octahedral positions [8,10]. Ferrite $ZnFe_2O_4$ at temperatures below the Neel point 9.5 K has a reverse spinel structure and is an antiferromagnet. At room temperature, zinc ferrite has a normal spinel structure and exhibits paramagnetic properties [8,11].

Various applications of SF required improvement of their magnetic characteristics, in particular, variation of their initial magnetic properties, for example, by doping with ions of other metals. As a result, SF $Co_{1-x}M_xFe_2O_4$ were created, Co ions in which are replaced by metal ions (M), which significantly changes the magnetic properties and structure of the initial ferrites. In the case of ferrite $CoFe_2O_4$, which has excellent magnetic characteristics, the reason for significant limitations for applications in biomedicine is its toxicity. Therefore, a number of works have been aimed at reducing the toxicity of MNP $CoFe_2O_4$, for example, by introducing non-toxic ions Zn [12–14] or Mn (see [14] and references there). In addition to reducing toxicity, Zn or Mn ions introduced into cobalt ferrite improve parameters for biomedical applications. Thus, the introduction of $CoFe_2O_4$ Zn ions from 5 to 15% (relative to Co) increases hyperthermic efficiency, but a further increase in the amount of Zn^{2+} leads to the opposite effect [15]. The maximum values of saturation magnetization (M_s), equal to ~ 90 and ~ 81 emu/g [16,17] respectively, were obtained for MNP of compositions $Co_{1-x}Zn_xFe_2O_4$ at $x \sim 0.4$ and when replaced in the $0.2 \leq x \leq 0.4$ area, the value of M_x was increased to ~ 100 emu/g, which suggests the prospects of these MNP for hyperthermic therapy [18]. The co-deposition-synthesized MNP $Co_{0.5}Zn_{0.5}Fe_2O_4$ have an almost spherical shape, which is important for magnetic hyperthermia [19].

The Mn-substituted particles $CoFe_2O_4$ ($Mn_{1-x}Co_xFe_2O_4$) are interesting because in addition to the nontoxicity of Mn ions, the mechanisms of substitution of iron ions by Mn ions in the structure of the SF are different. The occupancy of Co^{2+} nonequivalent positions in $Mn_{1-x}Co_xFe_2O_4$ ions were optimized [20] to increase the efficiency of heating by magnetic hyperthermia, and the particles are in the superparamagnetic state [14]. A decrease of the amount of Mn in $Mn_{1-x}Co_xFe_2O_4$ causes changes in the magnetic anisotropy and interparticle interactions, demonstrates the state of superspin glass [21], increases the ultrathin magnetic field in both sublattices by weakening the bonds $Fe^{3+}(A)-O-Fe^{3+}[B]$ [22], increases lattice parameters, average grain sizes, saturated magnetization [23,24].

It should be noted that a new unique method of combined therapy of malignant tumors (theranostics) is developed on the basis of SF MNP, combining diagnosis, targeted drug delivery and treatment [25]. In order to create SF combining the advantages of Zn and Mn ions, $Mn_{1-x}Zn_xFe_2O_4$ spinels were synthesized and studied, the synthesis methods of which and the magnetostructural characteristics are given in [26,27].

The most important result of the SF studies were the conclusions that the rearrangement of the magnetic properties of substituted SF is possible by changing the superexchange interactions of tetrahedral (A) and octahedral (B) positions depending on the distribution and ionic radii of cations [26,27]. The distribution of cations is influenced by synthesis methods, which makes it possible to control the properties and magnetic characteristics of ferrites.

SF doped with two or more metal ions [28–35] have become new for research and practical applications. The concentration of one of the substitutive elements is fixed in such SF, and the other two change within certain limits. Substitution of ferrite $Ni_{0.5}Zn_{0.5}Fe_2O_4$ with ions Cu^{2+}, Cd^{2+}, Co^{2+}, Ca^{2+} or Mn^{2+} leads to an increase in the crystal lattice constant, and the addition of nonmagnetic ions Mg, Cd and Ca reduces the saturation magnetization and T_C [28]. Saturation magnetization in CoZnMnFe ferrites$_2O_4$ decreases linearly with an increase of the content of Mn^{2+} ions; although with a small substitution of Mn T_C ions increases, but a further increase of the amount of Mn leads to a decrease of T_C [29]. Substitution of Zn^{2+} ions with Co^{2+} ions causes an increase in saturation magnetization and coercive force [30,31]. It was found from the Mössbauer data [31] that the ions Co^{2+} and Mg^{2+} prefer octahedral positions [B], and the ions Zn^{2+} predominantly occupy tetrahedral (A)-positions in $MgZnCoFe_2O_4$, whereas ions Fe^{3+} are randomly distributed at positions (A) and [B]. The saturation magnetization of particles $Mn_xCo_{0.5-x}Zn_{0.5}Fe_2O_4$ decreases with an increase in the concentration of Mn^{2+}, which is associated with a decrease in the size of the crystallites and the nonmagnetic nature of the Mn^{2+} [30] ions. The increase of the lattice constant in ferrites with an increase of Mn content is explained by the fact that the radius of Mn^{2+} ions is greater than the radius of Co^{2+} ions. A review of publications shows that the magnetic characteristics, such as saturation magnetization and coercive force, obtained as a result of substitution by ions of two metals, significantly exceed the parameters of the original unsubstituted ferrites or ferrites with one substituting ion. A strong dependence of the main magnetic parameters on the concentration of the alloyed element and the concentration ratios of the three substitutive components has also been established. Despite

the possibility of more subtle control of the properties of ferrites MFe_2O_4 when substituted with two metal ions, publications on studies of such substitutions are clearly insufficient.

Based on the above, MNP $Co_{0.8-x}Mn_xZn_{0.2}Fe_2O_4$ ($x = 0.6$, 0.4 and 0.2) were synthesized in this work and structural, microstructural, magnetic and hyperfine properties, the impact of the amount of Co and Zn ions introduced on the magnetic structure of particles, the dependence of magnetization on the distribution of cations over nonequivalent sublattices (A) and [B] were studied. X-ray diffraction and Mössbauer spectroscopy were used to study the structural, morphological and magnetic properties of synthesized ferrites.

2. Materials and methods

2.1. Synthesis of nanoparticle $Cos_{0.8-x}Mn_xZn_{0.2}Fe_2O_4$at $x = 0.6$, 0.4 and 0.2

Ferrite nanoparticles $Co_{0.8-x}Mn_xZn_{0.2}Fe_2O_4$ at $x = 0.6$, 0.4 and 0.2 were synthesized by single-stage co-deposition in an aquatic environment. The salts $MnCl_2$, $CoCl_{2.6}H_2O$, $ZnCl_2$ and $FeCl_3$ in the required amount for each composition were dissolved in 200 ml of water and heated at constant stirring up to 80°C. The pH value of the mixture was set in the range from 12 to 13, by adding drops of NaOH solution with constant stirring. The resulting mixture was kept at 85°C for 1 hr, then cooled to room temperature and the resulting powders were washed using a centrifuge at 8000 rpm. Synthesized nanoparticles dried under an IR lamp were used for the study.

2.2. Characterization of nanoparticles $Co_{8-x}Zn_xMn_{0.2}Fe_2O_4$

The structure, phase state and particle sizes were determined using profile of X-ray diffractograms (XRD) obtained using a D8 ADVANCE Bruker XRD diffractometer using Cu-Kα-radiation with a wavelength of 1.542 Å. Magnetic measurements in a constant magnetic field were carried out using vibrating sample magnetometer (VSM) of the Physical Properties Measurement System (PPMS) from Quantum Design.

To investigate magnetic properties and magnetic structure, the Mössbauer spectroscopy was applied, which is an informative method of studying properties of materials [36–38]. The Mössbauer spectra (MS) were acquired using the isotope ^{57}Fe with registration in the geometry of transmittance of the radiation from ^{57}Co source through the studied sample γ- in the rhodium matrix (Rh). The reference signal in the system of motion of the Doppler modulator in the spectrometer had a shape of triangle to set a speed with constant acceleration. The speed scale was calibrated using iron α-foil at room temperature, and for a higher accuracy the calibration was carried out using a laser interferometer. The MS of investigated samples were obtained at room temperature. The spectra were mathematically processed by a program [39] that describes spectral lines by Lorentz shape peaks using the least square method. The program implements the search for optimal values on the speed scale of the parameters of spectral lines in the procedure for minimizing the functional $\chi 2$, namely, widths, intensities and positions. The parameters of hyperfine interactions (HFI) are calculated using the positions of the lines: IS — isomeric chemical shift, QS — quadrupolar splitting, H_{eff} — effective magnetic field.

The use of Lorentz lines for MS processing in order to study the distribution of the effective magnetic field $P(H_{\text{eff}})$ arising from the local inhomogeneity of the distribution of cations is not effective if sixtuplets are not resolved. Therefore, the field distribution functions $P(H_{\text{eff}})$ were reconstructed from experimental MNP MS using the program [39] describing MS with Voigt lines.

3. Results and discussion

3.1. X-ray diffraction analysis of MNP $Co_{0.8-x}Mn_xZn_{0.2}Fe_2O_4$

Radiographs of synthesized nanoparticles $Co_{0.8-x}Mn_xZn_{0.2}Fe_2O_4$ are shown in Fig. 1, *a*. The diffraction peaks belonged to the ferrite phase without additional peaks corresponding to the impurity phases ZnO, MnO_2, Fe_2O_3 and CoO, possible due to the precursors used [40]. The average sizes of the crystallites were calculated from the half-width of the peak of the highest intensity (311) using the Scherrer formula [40]. The values of the lattice constants of mixed ferrite nanoparticles were determined by fitting and refining multiple peaks using the Jade-XRD software. The average lattice sizes and parameters are given in Table 1. CM-06 nanoparticles with a high concentration of Mn^{2+} have larger sizes compared to CM-04 and CM-02 MNP. The shift of the peak position depending on the composition is shown in Fig. 1, *b*. The peaks for particles with a high concentration of Mn^{2+} (CM-02) are shifted towards a smaller diffraction angle due to the larger lattice size. The permanent lattices of the studied nanoparticles were compared with the lattice parameters of ferrites without substitution, also obtained by a similar method of co-deposition: $MnFe_2O_4$ (8.4889 Å) [20], $CoFe_2O_4$ (8.3891 Å) [20] and $ZnFe_2O_4$ (8.3970 Å) [42]. A decrease of the lattice constant of nanoparticles of mixed structure is expected with an increase in the concentration of Co^{2+} since the radius of the ions Co^{2+} is smaller than that of Mn^{2+}.

3.2. Mössbauer studies of MNP $Co_{0.8-x}Mn_xZn_{0.2}Fe_2O_4$

The Mössbauer spectroscopy provides an unique information on the phase composition, local electron configurations, magnetic structure and phenomena of magnetic relaxation

Table 1. Average crystallite sizes and constant ferrite lattices $Co_{0.8-x}Mn_xZn_{0.2}Fe_2O_4$ ($x = 0.6$, 0.4, 0.2)

MNP composition	Average size, nm	Lattice constant, Å	References
$Co_{0.2}Mn_{0.6}Zn_{0.2}Fe_2O_4$ ($x = 0.6$)	15.2	8.4353	This study
$Co_{0.4}Mn_{0.4}Zn_{0.2}Fe_2O_4$ ($x = 0.4$)	10.2	8.4206	This study
$Co_{0.6}Mn_{0.2}Zn_{0.2}Fe_2O_4$ ($x = 0.2$)	10.3	8.3963	This study
$MnFe_2O_4$	34.9	8.4889	[20]
$CoFe_2O_4$	15.0	8.3891	[20]
$ZnFe_2O_4$	11.0	8.4280	[42]

of nanosize systems [36–38]. MS of MNP ^{57}Fe ferrite $Co_{0.8-x}Mn_xZn_{0.2}Fe_2O_4$, registered at room temperature, are shown in Fig. 2. The experimental values in Fig. 2 are shown by dots, and the model values obtained by mathematical processing of MS using the program [39] are shown by solid lines. As can be seen in Fig. 2, MS of MNP $Co_{0.8-x}Mn_xZn_{0.2}Fe_2O_4$ at $x = 0.6$ and 0.2 consist of lines of Zeman sextiplets (ZS), asymmetric in the direction of zero line speeds. A doublet is observed against the background of the ZS in the region of zero velocities at $x = 0.4$. It should be noted that the experimental MS MNP (Fig. 2) are similar to the spectra of substituted spinel ferrites obtained in [10,14,16,29–31,33,35,37,38,41,43–53].

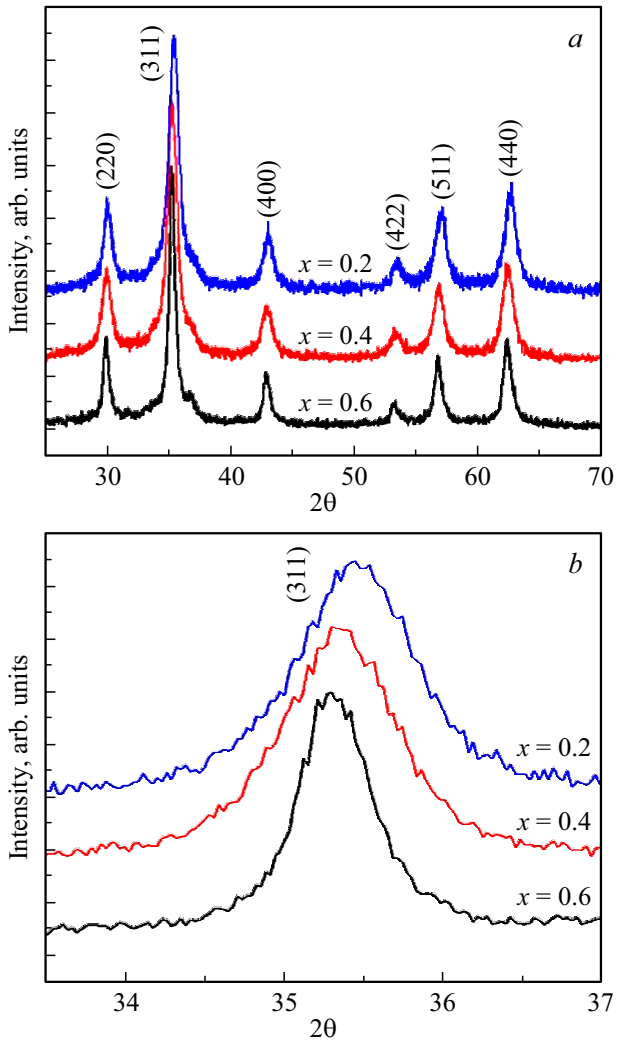

Figure 1. *a*) X-ray diffractograms of nanoparticles $Co_{0.8-x}Mn_xZn_{0.2}Fe_2O_4$. *b*) Maximum intensity peak offset (311) depending on the composition of ferrite $Co_{0.8-x}Mn_xZn_{0.2}Fe_2O_4$

The analysis of experimental MS (Fig. 2) is based on the following. The iron ion in the tetrahedral node (A) is surrounded by 12 ions of octahedral [B]-positions in MNP of spinel ferrites MFe_2O_4. Substituting one [B]-ion Fe^{3+} with M^{2+} does not significantly change the total super-exchange interaction to cause a noticeable difference in the effective fields of Fe(A) ions sublattices, and the Zeeman component of ions Fe^{3+}(A) sublattices are described by one ZS. Ultrathin magnetic fields on the nuclei of Fe ions at position [B] are formed by six nearest neighbors (A)-ions, which can be occupied by both ions Fe^{3+} and ions M^{2+}. The weight of the different ZS ions of the Fe[B]-sublattice is proportional to the probability of different environments, so it can be calculated under the assumption that the Fe and M ions are randomly distributed over (A)-positions. The probability that the Fe ions in the [B]-positions are surrounded by the nearest (A) neighbors is calculated by the binomial distribution of n Fe ions and $(6 - n)M$ —metal ions [54]. In this case, the cation Fe^{3+} in the [B]-position is surrounded by 6 cations as follows: $6Fe^{3+}$, $5Fe^{3+} + 1Mg^{2+}$ and $4Fe^{3+} + 2Mg^{2+}$, and etc. [49,50]. Since the iron ion in the [B]-position is surrounded by six nearest neighbors of the ions in the (A)-positions, the substitution of one ion Fe^{3+} in the (A)-node by the ion M^{2+} leads to a noticeable change in super-exchange interactions. In other words, a change in the distribution of cations in the [B]-positions by only 1/12 part affects the (A)-positions, whereas a change in the distribution of cations in the (A)-positions leads to changes in the [B]-sublattice by 1/6. Consequently, the change of the number of Fe and M^{2+} ions in the immediate environment of Fe ions in [B]-nodes, the effective magnetic field and the intensity of absorption lines for different environments of [B]-iron ions varies. This leads to an asymmetric broadening of the ZS lines towards the center of the spectrum, which is observed at experimental MS.

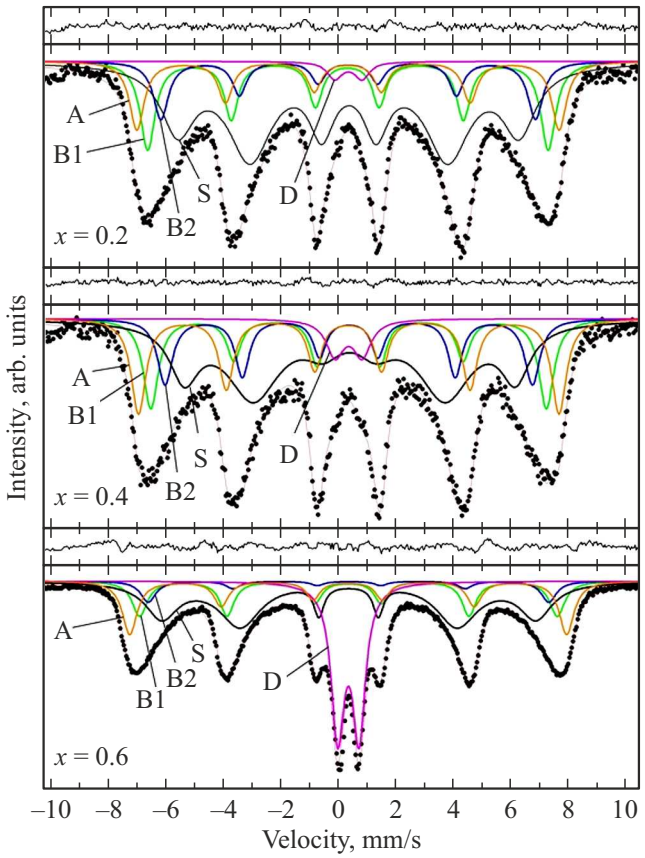

Figure 2. Mössbauer spectra of MNP $Co_{0.8-x}Mn_xZn_{0.2}Fe_2O_4$ at $x = 0.6$, 0.4 and 0.2, acquired at room temperature. The experimental values are shown by dots and the model components are shown by solid colored lines. The sextiplet denoted as A refers to Fe ions in (A)-positions, B — to Fe ions in [B]-positions, D — paramagnetic doublet. Sextiplets S belong to Fe ions occupying positions in the surface layer.

In the studied MNP $Co_{0.8-x}Mnx Zn_{0.2}Fe_2O_4$ the presence of four different cations (iron, cobalt, zinc and manganese) significantly increases the chances of their random distribution, which also leads to the formation of several unequal positions differing in population, as observed in [50]. Therefore, a model consisting of six ZS (one — for Fe [A]-position ions, five — for Fe ions in [B]-positions having different environments) was initially used for mathematical processing of experimental MS of MNP $Co_{0.8-x}Mn_xZn_{0.2}Fe_2O_4$. However, this model was not consistent with experimental MS. As a result, when selecting a model to describe experimental spectra, it was found that four ZS and one doublet allow satisfactorily describing experimental spectra according to the criteria of the smallest values $\chi 2$, which are within 1.0−1.2, as well as the minimum difference between the model and experimental values shown in Fig. 2 above each spectrum. The HFI parameters presented in Table 2 are calculated from the positions of the spectral lines in MNP MS (Fig. 2). The IS values are given relative to the metal foil α-Fe.

Impurity phases in the amount of more than 3 at.% of iron appear on MS as additional ZS or doublets. No secondary phase lines were detected during the analysis of the MNP MS (Fig. 2), which indicates the absence of impurities in the studied particles and is consistent with the data of the XRD. QS values (except QS for doublets, table 2) the nonequivalent positions of iron ions in the studied MNP are close to zero within the experimental error, which indicates the preservation of the cubic symmetry of the ions Fe^{3+} and their environment.

The relation of spectral lines in Mössbauer spectroscopy with the ions Fe^{2+} and Fe^{3+} is reliably identified by their chemical shifts amounting to $\sim 0.2-0.5$ mm/s for Fe^{3+} and $\sim 0.9-1.1$ mm/s for Fe^{2+} [14]. In the case of SF MNP, the IS values belonging to iron ions in the high-spin state Fe^{3+}, as a rule, are within the range of 0.3−0.6 mm/s. As can be seen from Table 2, the IS values of Fe ions in [B]- and (A)-positions practically coincide and do not depend on the number of Mn ions, which indicates the insensitivity of the s-electrons of the ions Fe^{3+} to the quantity of Zn and Mn. There are no high values of chemical shifts (from 0.9 to 1.1 mm/s) belonging to Fe ions in the low-spin state Fe^{2+} indicating that only iron ions in the high-spin state Fe^{3+} are present in the studied MNP.

One of the tasks of Mössbauer spectroscopy is to correlate ZS with Fe ions in the corresponding positions (A) and [B]. It is stated in [56] that the sextiplets in the SF MFe_2O_4 with the largest values IS and H_{eff} belong to the ions Fe^{3+} in octahedral [B]-ions, surrounded by six nearest ions Fe^{3+}. The sextiplet, with a lower IS value and H_{eff} belongs to the ions of Fe^{3+} tetrahedral positions (A) [56]. However, as can be seen from Table 2, the values of IS for iron ions in (A)- and [B]-positions coincide within the error. Calculations showed that the covalence of the Fe(A)−O bond is higher than that of Fe[B]−O, which qualitatively explains why the transfer of spin density from (A)- to [B]-ions in the spinel structure is more efficient, than the transfer in the reverse direction [54]. A number of studies showed that the ultrathin magnetic field of Fe ions in (A)-nodes in the SF MFe_2O_4 is greater than in the nodes [B] [23,43,52,54,57–59]. Therefore, the relation of ZS (Fig. 2) to the iron ions of (A)- and [B]-sublattices was determined using the value of H_{eff}. The sextiplet with the largest value H_{eff} are related to Fe ions in (A)-nodes, sextiplets with successively decreasing fields are related to Fe ions occupying positions [B1], [B2], as shown in Fig. 2.

MNP MS at $x = 0.4$ (Fig. 2) consists of the lines of the ZS, doublet and asymmetric in the direction of zero velocities of the lines ZS. The presence of a doublet on the MS can be explained by the existence of a size distribution in the MNP. Particles of the smallest sizes have paramagnetic state at temperatures lower than larger particles, and the relaxation time τ of smaller nanoparticles is less than the measurement time by Mössbauer spectroscopy ($\tau_{\text{M}} = 10^{-7}$ s for ^{57}Fe); then there is a doublet on the MS. Such a state of particles is called superparamagnetic [60–62]. At $\tau \gg \tau_{\text{M}}$, MS consists of ZS with a good resolution

Table 2. Widths of the first lines (G) of the Zeeman splitting, as well as isomeric shifts (IS), quadrupolar splitting (QS), effective magnetic fields (H_{eff}) and areas of lines (In) of Fe ions in tetraheric (A), octahedral [In] positions, in the surface layer (S) and doublets (D) for MNP $Co_{0.8-x}Mn_xZn_{0.2}Fe_2O_4$

x	Component	Width G, mm/s	IS, mm/s	QS, mm/s	H_{eff}, kOe	In, %
0.2	A	0.620 + / − 0.000	0.313 + / − 0.008	0.006 + / − 0.015	455.4 + / − 0.07	14
	B1	0.630 + / − 0.000	0.306 + / − 0.006	0.021 + / − 0.012	432.1 + / − 0.07	19
	B2	0.637 + / − 0.000	0.320 + / − 0.010	0.009 + / − 0.020	404.0 + / − 0.11	11
	S	1.393 + / − 0.063	0.340 + / − 0.008	0.017 + / − 0.015	368.0 + / − 0.18	54
	D	0.619 + / − 0.107	0.330 + / − 0.000	0.936 + / − 0.000	–	2
0.4	A	0.622 + / − 0.000	0.323 + / − 0.005	0.021 + / − 0.010	454.1 + / − 0.05	21
	B1	0.629 + / − 0.000	0.327 + / − 0.007	0.002 + / − 0.015	427.1 + / − 0.08	17
	B2	0.630 + / − 0.000	0.333 + / − 0.007	0.001 + / − 0.015	396.7 + / − 0.10	15
	S	1.223 + / − 0.082	0.360 + / − 0.013	0.023 + / − 0.022	357.5 + / − 0.21	43
	D	0.746 + / − 0.074	0.330 + / − 0.000	0.936 + / − 0.000	–	4
0.6	A	0.616 + / − 0.000	0.317 + / − 0.003	0.016 + / − 0.006	471.3 + / − 0.02	17
	B1	0.625 + / − 0.000	0.326 + / − 0.003	0.013 + / − 0.006	450.5 + / − 0.04	16
	B2	0.631 + / − 0.000	0.345 + / − 0.012	0.020 + / − 0.025	432/1 + / − 0.084	6
	S	1.361 + / − 0.025	0.342 + / − 0.003	0.007 + / − 0.006	403.6 + / − 0.05	38
	D	0.538 + / − 0.003	0.330 + / − 0.000	0.733 + / − 0.000	–	23

of Zeeman absorption lines by Fe ions in nonequivalent sublattices [60–62].

The analysis of MNP MS (Fig. 2) showed that for the best compliance with experimental MS, it is necessary to introduce a sextiplet, indicated in Fig. 2 as S. The difference between the effective fields of the sextiplets S and [B1] is noticeably greater than the difference of the fields between ZS [B1] and [B2] (Table 2). It is also characteristic that the line widths of the sextiplet S are twice as wide as the line widths of the ZS ions of Fe (A)- and [B]-positions. Similar MNP MS of substituted SF with asymmetrically widened lines are published in [10,14,16,29–31,33,35,37,38,43–53], but the reasons for the formation of such spectra were explained in different ways. For example, the presence of such sextiplets was explained by an increase in particle sizes and impurity phases at high annealing temperatures [46]. The MS sextiplet in [64] with good resolution was attributed to larger particles in the sample with magnetic ordering, for which $\tau \gg \tau_{\text{M}}$, and the MS with wide unresolved lines was attributed to smaller particles in the superparamagnetic state ($\tau \ll \tau_{\text{M}}$). However, it is unlikely that two groups of particles of different sizes are present in single-phase samples with well-crystallized particles, which was also refuted by X-ray diffraction analysis. The presence of ZS with asymmetrically widened lines on MS in [12] was explained by the random distribution of ions Fe^{3+} and Zn^{2+} at the (A)-position, and this ZS was attributed to Fe^{3+} [B]-ions having a smaller number of magnetic ions in (A) positions. However, even the absence of five magnetic ions in (A)-positions surrounding [B]-ions is not able to reduce the effective fields by such a large amount (see Table 2). It was suggested in [12] that sextiplets showing smaller hyperfine fields and wide lines refer to Fe ions located on the surface of the MNP. It has also been suggested that a „magnetically dead“ layer [63,64], a spin-glass layer [49], a layer with a canting spin structure [59,60] are formed on the surface of the particles, lowering the saturation magnetization and the temperature of the magnetic ordering of MNP. Spin glass state observed on the surface [49] does not contribute to the magnetism of particles; perhaps that is why such a surface layer was called „magnetically dead“ [63,64].

Thus, all explanations were justified by the exclusive role of the surface. It should be noted that the model of the skewed state of spins was described in [65]. The existence of an anisotropic layer on the surface in ferromagnetic crystals was theoretically predicted by L. Neel in 1954 [66]. However, experimental studies of the structure and properties of the surface layer attracted attention much later (see [67,68] and references there). Thin films and nanoscale powders were used for these purposes, because the surface/volume ratio increases many times in these materials and the surface spins of Fe ions become dominant in the magnetic properties of the entire particle. The existence of a canting state of spin moments on the surface of particles was first proved using strong magnetic fields

in the Mössbauer studies [69], and a model of the type „core–shell" was proposed. In such a model, it is assumed that the MNP consists of a central part (core), with a ferromagnetic (collinear) ordering of spins, and a surface layer (shell) in which the spins are non-collinear to each other (canting structure) [69,70]. In the future, this model was also confirmed by Mössbauer studies in large external magnetic fields (see [70] and references there).

However, the heterogeneity of the ensemble of particles in size, superparamagnetic phenomena, strong dependence on the preparation technology, etc. significantly complicated the task of studying the properties of the surface on the example of fine powders. All these difficulties are addressed by the use of macroscopic crystals, however, there were no techniques that allow studying the properties of the surface layer of macrocrystals in direct comparison with the properties of the volume.

The „method of simultaneous gamma-ray, X-ray and electron Mössbauer spectroscopy (SGXEMS) provided new perspectives in the study of the properties of the surface of macroscopic crystals", the idea of which was first proposed and implemented by the authors in the form of an automated system [71–73]. The uniqueness of the SGXEMS method is that information about the state of the surface layer and the volume of the crystal is extracted simultaneously using the same technique (Mössbauer spectroscopy), which allows for a direct comparison of experimental data of the properties of the surface and the volume of the crystal. Later, the SGXEMS method in foreign literature was called „Simultaneous Triple Radiation Mössbauer Spectroscopy (STRMS)" [74,75].

The SGXEMS method was used to obtain the first direct experimental confirmation of the existence in macroscopic crystals of Fe_3BO_6 „of a transitional" surface layer, within which the angle of deviation of the magnetic moments of iron ions from orientation in the volume increases smoothly as they approach the surface [67,68]. The SGXEMS method did not detect, „the transition" surface layer in hexagonal ferrites of the type M ($BaFe_{12}O_{19}$, $SrFe_{12}O_{19}$, $PbFe_{12}O_{19}$) because, as the analysis of model MS showed, the thickness of such a layer in these hexaferrites cannot exceed units of nm [76]. This is significantly less than the accuracy of the experiment, which is ~ 10 nm, but coincides with the value obtained from theoretical calculations by L. Neel [66]. However, the thickness of the „transition" layer increases in case of introduction of a small amount of diamagnetic ions Sc into hexaferrite type Ba–M (chemical formula $BaFe_{12-x}Sc_xO_{19}$), or Al ions in Sr–M ($SrFe_{12-x}Al_xO_{19}$), replacing iron ions due to the breakage of super-exchange bonds, both due to the surface and diamagnetic ions, and reaches ~ 200 nm [67,77–80] respectively. Consequently, the surface and diamagnetic ions lead to significant changes in the super-exchange interactions of iron ions occupying positions in the surface and near-surface layers. It can be argued that the deviation of the orientation of the moments observed in the surface layer of macrocrystals from the direction in the volume [67,73,74] should be preserved when the size of the macrocrystals decreases to nanowires,

Table 2 shows that the difference of the values of H_{eff} [B]-sublattice and sextiplet S is significantly greater at $x = 0$ and 0.25 than in case of substitution of the immediate environment [B]-ions of one Fe ion with a diamagnetic one [54]. The large line widths of the S component and the large difference in the effective fields of the S- and [B]-sextiplets suggest that the S sextiplet is formed by iron ions located on the surface and in the subsurface layer of MNP, in which the presence of the surface led to the loss of more magnetic neighbors and, consequently, super-exchange bonds than in ions in the volume of the particle. An additional contribution to the sextiplet S may be from the same Fe ions of the surface and near-surface layer, which, due to the loss of part of the super-exchange interactions, pass into the superparamagnetic state at temperatures lower than the ions in the volume of the particle [60–62].

It should be noted that the state with different magnetic structures of the volume and the surface layer in the SF MNP cannot be observed by other methods other than Mössbauer spectroscopy. This is explained by the fact that SF MNP are single-phase, well crystallized, and consist of a single material. This distinguishes SF particles from core/shell composites, in which the core and shell are made of different magnets, for example, magnetite and maghemite [81]. Thus, for the first time without the use of high magnetic fields (expensive equipment), using the example of SF nanoparticles $Co_{0.8-x}Mn_xZn_{0.2}Fe_2O_4$ it is shown that the volume and surface layer of particles have different magnetic structures, and like in [69] such particles can be called MNP of the core–shell type.

3.3. Distribution functions of effective magnetic fields $P(H_{\text{eff}})$ in MNP $Co_{0.8-x}Mn_xZn_{0.2}Fe_2O_4$ ($x = 0.6$, 0.4 and 0.2)

The study of the distribution of the effective magnetic field $P(H_{\text{eff}})$ arising from the local inhomogeneity of the distribution of cations by modeling poorly resolved MS Lorentz lines is not effective. In this case, the most reliable is the MS analysis with the description of spectral lines by the Voigt function [82,83]. Therefore, the field distribution functions $P(H_{\text{eff}})$ presented in Fig. 3 were reconstructed from experimental MNP MS $Co_{0.8-x}Mn_xZn_{0.2}Fe_2O_4$ (Fig. 2) using the program [39] describing MS with Voigt lines. The obtained $P(H_{\text{eff}})$ functions differ from the curve $P(H_{\text{eff}})$ of SF macrocrystals, where two maxima belonging to iron ions are observed in two nonequivalent sublattices (A) and [B].

A line is observed on the functions $P(H_{\text{eff}})$ obtained for MNP (Fig. 3) in the field range from 25 to 55 T, that is asymmetric in the direction of smaller field values. Mathematical processing of the line observed in the range from 25 to 55 T, showed that it can be described by four peaks, shown in Fig. 3 arrows and marked A, B1, B2 and S, confirming that these lines belong to the corresponding ZS,

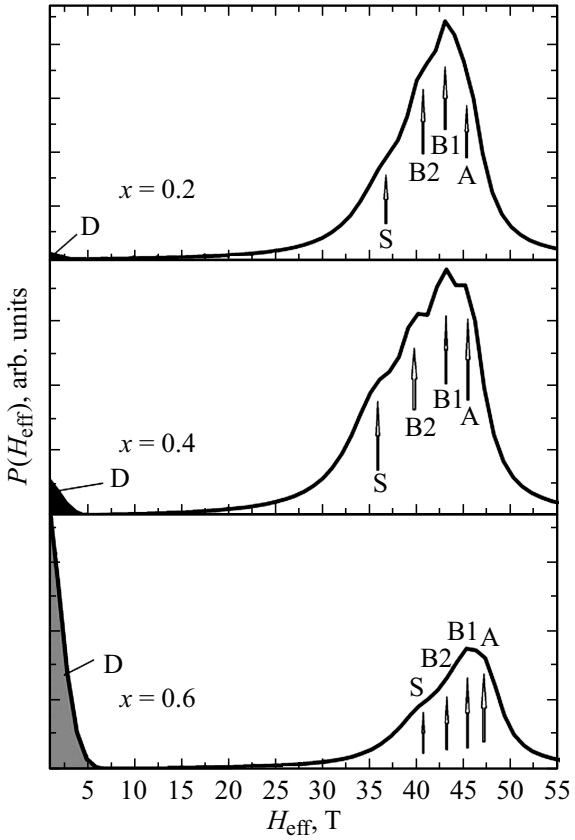

Figure 3. Distribution functions of effective magnetic fields $P(H_{\text{eff}})$, reconstructed from experimental MNP MS $Co_{0.8-x}Mn_xZn_{0.2}Fe_2O_4$ using the program [39].

as discussed above. The region from 0 to 5 T corresponds in MS to doublet lines related to the fraction of particles in the paramagnetic state, the probability of their presence is different for different compositions, as indicated by different intensities of this line.

Thus, the functions $P(H_{\text{eff}})$ (Fig. 3) reflect the complex magnetic structure of the studied MNP, which cannot be explained only by the statistical distribution of ions surrounding iron ions, but it is necessary to take into account the significant influence of the surface, which increases with the decrease of particles to nanometer sizes.

4. Conclusion

Systematic studies were conducted in MNP $Co_{0.8-x}Mn_xZn_{0.2}Fe_2O_4$ ($x = 0.6$, 0.4 and 0.2) structural and exchange interactions depending on the concentration of Zn ions, with a fixed amount of Mn. The particles were synthesized using a co-deposition method. The structural and morphological properties of MNPs were studied using X-ray diffraction and Mössbauer spectroscopy. Structural XRD analysis confirms that the studied particles are single-phase and in the studied range of substitution with Mn ions have a cubic structure of SF (spatial group Fd3m). The sizes of $Co_{0.8-x}Mn_xZn_{0.2}Fe_2O_4$nanoparticles calculated using radiographs are 15.2, 10.2 and 10.3 nm at $x = 0.6$, 0.4 and 0.2 respectively.

Mössbauer studies showed differences between the magnetic structure of the volume and the surface layer, for the first time without the use of strong magnetic fields, based on the example of SF ferrite nanoparticles $Co_{0.8-x}Mn_xZn_{0.2}Fe_2O_4$ ($x = 0.6$, 0.4 and 0.2). In the body of particles, a collinear ordering of spin moments is observed, whereas in the surface layer spin moments have a canting structure due to the loss of part of the super-exchange interactions. Consequently, MNPs $Co_{0.8-x}Mn_xZn_{0.2}Fe_2O_4$ are formed as particles of the core–shell type, the inner part of which (the core) has a magnetic Neel ordering, whereas there is a canted orientation of moments on the surface of the particles (the shell).

The obtained MNPs of spinel ferrites $Co_{0.8-x}Mn_xZn_{0.2}Fe_2O_4$ ($x = 0.6$, 0.4 and 0.2), and also, the research results are important for the development and creation of magnetic nanoparticles for various applications, including biomedical ones, because it is shown that to improve the magnetic properties of ferrite nanoparticles, the structure of moments in the surface layer should be controlled.

Acknowledgments

B. Issa would like to thank the University of Sharjah and the Sharjah Research Academy for grant No. 2101050262 for joint research activities.

Conflict of interest

The authors declare that they have no conflict of interest.

References

[1] G. Sharma, A. Kumar, P. Dhiman. Ferrites — Nanostructures with Tunable Properties and Diverse Application. Materials Research Forum LLC, USA (2021). 374 p.
[2] X. Liu, Y. Zhang, Y. Wang, W. Zhu, G. Li, X. Ma, Y. Zhang, S. Chen, S. Tiwari, K. Shi, S. Zhang, H. M. Fan, Y. X. Zhao, X.-J. Liang. Theranostics **10**, *8*, 3793 (2020).
[3] A. Rajan, N.K. Sahu. J. Nanopart. Res. **22**, *11*, 319 (2020).
[4] B. Issa, I.M. Obaidat. In: Magnetic Resonance Imaging / Ed. L. Manchev. InTechOpen (2019). Ch. 2. http://dx.doi.org/10.5772/intechopen.84649
[5] B. Pacakova, S. Kubickova, A. Reznickova, D. Niznansky, J. Vejpravova. In: Magnetic Spinels — Synthesis, Properties and Applications / Ed. M.S. Seehra. InTechOpen (2017). Ch. 1, pp. 4–29. https://www.intechopen.com/chapters/52889
[6] Y. Xiao, J. Du. J. Mater. Chem. B **8**, *3*, 354 (2020).
[7] S. Amiri, H. Shokrollahi. Mater. Sci. Eng. C **33**, *1*, 1 (2013). https://doi.org/10.1016/j.msec.2012.09.003

[8] K.K. Kefeni, T.A.M. Msagati, T.T. Nkambule, B.B. Mamba. Mater. Sci. Eng. C **107**, 110314 (2020). https://doi.org/10.1016/j.msec.2019.110314
[9] A. Manohar, D.D. Geleta, C. Krishnamoorthi, J. Lee. Ceram. Int. **46**, *18*, 28035 (2020).
[10] M. Popa, P. Bruna, D. Crespo, J.M. Calderon Moreno. J. Am. Ceram. Soc. **91**, 2488 (2008). https://ceramics.onlinelibrary.wiley.com/doi/abs/10.1111/j.1551-2916.2008.02501.x
[11] O. Perales-Pérez, Y. Cedeño-Mattei. In: Magnetic Spinels — Synthesis, Properties and Applications / Ed. M.S. Seehra. InTechOpen (2017). Ch. 3. P. 51–72. https://www.intechopen.com/chapters/53689
[12] F. Nakagomi, P.E.N. de Souza, T.J. Castro, V.K. Garg, A.C. Oliveira, F.C.E. Silva, A. Franco Jr., P.C. Morais, S.W. da Silva. J. Alloys. Compd. **842**, 155751 (2020).
[13] F. Sharifianjazi, M. Moradi, N. Parvin, A. Nemati, A.J. Rad, N. Sheysi, A. Abouchenari, A. Mohammadi, S. Karbasi, Z. Ahmadi, A. Esmaeilkhanian, M. Irani, A. Pakseresht, S. Sahmani, M.S. Asl. Ceram. Int. **46**, *11*, Part B, 18391 (2020).
[14] A.S. Kamzin, I.M. Obaidat, V.G. Semenov, V. Narayanaswamy, I.A. Al-Omari, B. Issa, I.V. Buryanenko. FTT **64**, *6*, 712 (2022). https://journals.ioffe.ru/articles/52406 [A.S. Kamzin, I.M. Obaidat, V.G. Semenov, V. Narayanaswamy, I.A. Al-Omari, B. Issa, I.V. Buryanenko. Phys. Solid State **64**, *6*, 698 (2022). https://journals.ioffe.ru/articles/53838].
[15] M. Albino, E. Fantechi, C. Innocenti, A. López-Ortega, V. Bonanni, G. Campo, F. Pineider, M. Gurioli, P. Arosio, T. Orlando, G. Bertoni, C. De Julián Fernández, A. Lascialfari, C. Sangregorio. J. Phys. Chem. C **123**, *10*, 6148 (2019). https://doi.org/10.1021/acs.jpcc.8b10998
[16] V. Mameli, A. Musinu, A. Ardu, G. Ennas, D. Peddis, D. Niznansky, C. Sangregorio, C. Innocenti, N.T.K. Thanh, C. Cannas. Nanoscale **8**, *19*, 10124 (2016). https://pubs.rsc.org/en/content/articlelanding/2016/nr/c6nr01303a
[17] A. Ramakrishna, N. Murali, T.W. Mammo, K. Samatha, V. Veeraiah. Physica B: Condens. Matter **534**, 134 (2018). https://doi.org/10.1016/j.physb.2018.01.033
[18] T. Dippong, O. Cadar, E.A. Levei, I.G. Deac. J. Magn. Magn Mater. **498**, 166168 (2020). https://doi.org/10.1016/j.jmmm.2019.166168
[19] A.S. Kamzin, D.S. Nikam, S.H. Pawar. Phys. Solid State **59**, *1*, 156 (2017). https://link.springer.com/article/10.1134/S1063783417010127.
[20] V. Narayanaswamy, I.A. Al-Omari, A.S. Kamzin, B. Issa, H.O. Tekin, H. Khourshid, H. Kumar, A. Mallya, S. Sambasivam, I.M. Obaidat. Nanomater. **11**, *5*, 1231 (2021). https://doi.org/10.3390/nano11051231
[21] B. Aslibeiki, P. Kameli, H. Salamati, G. Concas, M.S. Fernandez, A. Talone, G. Muscas, D. Peddis. Beilstein J. Nanotechnol. **10**, 856 (2019). https://www.beilstein-journals.org/bjnano/articles/10/86
[22] R. Roongtao, R. Baitahe, N. Vittayakorn, P. Seeharaj, W.C. Vittayakorn. Ferroelectrics **459**, *1*, 119 (2014). https://www.tandfonline.com/doi/abs/10.1080/00150193.2013.849175
[23] S.P. Yadav, S.S. Shinde, P. Bhatt, S.S. Meena, K.Y. Rajpure. J. Alloys Compd. **646**, 550 (2015). http://dx.doi.org/10.1016/j.jallcom.2015.05.270
[24] A. Farheen, R. Singh. Integrated Ferroelectrics **203**, *1*, 91 (2019). https://doi.org/10.1080/10584587.2019.1674960
[25] M.F.A. Khan, M.D.F. Ahammad, N.H. Khan, N. Ahmed. Austin J. Pharmacol Therap. **9**, *5*, 1150 (2021).
[26] P. Thakur, D. Chahar, S. Taneja, N. Bhalla, A. Thakur. Ceram. Int. **46**, *10*, Part B, 15740 (2020). https://doi.org/10.1016/j.ceramint.2020.03.287
[27] F. Khan, B.B. Lahiri, S. Ranoo, J. Philip. Ceram. Int. **48**, *22*, 33462 (2022). https://doi.org/10.1016/j.ceramint.2022.07.291
[28] E. Rezlescu, L. Sachelarie, P.D. Popa, N. Rezlescu. IEEE Trans. Magn. **36**, *6*, 3692 (2000). https://ieeexplore.ieee.org/document/914348
[29] I. Sharifi, H. Shokrollahi. J. Magn. Magn. Mater. **334**, 36 (2013). https://doi.org/10.1016/j.jmmm.2013.01.021
[30] M. Hashim, S.S. Meena, R.K. Kotnala, S.E. Shirsath, P. Bhatt, S. Kumar, E. Şentü rk, R. Kuma, N. Gupta, Alimuddin. J. Magn. Magn. Mater. **360**, 21 (2014). http://dx.doi.org/10.1016/j.jmmm.2014.01.047
[31] M. Hashim, S.S. Meena, D. Ravinder, R. Kumar, P. Bhatt, S. Kumar, Alimuddin. AIP Conf. Proc. **1591**, 1533 (2014).
[32] G. Kumar, R.K. Kotnala, J. Shah, V. Kumar, A. Kumar, P. Dhiman, M. Singh. Phys. Chem. Chem. Phys. **19**, *25*, 16669 (2017).
[33] M.A. Ahmed, H.E. Hassan, M.M. Eltabey, K. Latka, T.R. Tatarchuk. Physica B: Phys. Condens. Matter **530**, 195 (2018). https://doi.org/10.1016/j.physb.2017.10.125
[34] H. Mahajan, S.K. Godara, A.K. Srivastava. J. Alloys. Compd. **896**, 162966 (2022). https://doi.org/10.1016/j.jallcom.2021.162966
[35] S. Dlamini, S. Nkosi, T. Moyo, A. Nhlapo. Mater. Sci. Eng. B **294**, 116554 (2023).
[36] Applications of Mössbauer Spectroscopy. 1st ed. / Ed. R.L. Cohen. Elsevier (1980).
[37] V. Kuncser, O. Crisan, G. Schinteie, F. Tolea, P. Palade, M. Valeanu, G. Filoti. Modern Trends in Nanoscience. Editura Academiei Romane, Bucharest (2013). V. 197.
[38] A.S. Kamzin, I.M. Obaidat, V.G. Semenov, V. Narayanaswamy, I.A. Al-Omari, B. Issa, I.V. Buryanenko. Phys. Solid State **65**, *3*, 470 (2023). https://journals.ioffe.ru/articles/55591.
[39] V.G. Semenov, V.V. Panchuk. MÖssbauer Spectra Processing Software MossFit. Private message.
[40] H.L. Andersen, C. Granados-Miralles, M. Saura-Muzquiz, M. Stingaciu, J. Larsen, F. Søndergaard-Pedersen, J.V. Ahlburg, L. Keller, C. Frandsen, M. Christensen. Mater. Chem. Front. **3**, *4*, 668 (2019).
[41] A.P. Kazin, M.N. Rumyantseva, V.E. Prusakov, I.P. Suzdalev, A.M. Gaskov. Inorg. Mater. **48**, *5*, 525 (2012). https://link.springer.com/article/10.1134/S002016851205007X.
[42] M.A.A. Kerroum, A. Essyed, C. Iacovita, W. Baaziz, D. Ihiawakrim, O. Mounkachi, M. Hamedoun, A. Benyoussef, M. Benaissa, O. Ersen. J. Magn. Magn. Mater. **478**, 239 (2019). https://doi.org/10.1016/j.jmmm.2019.01.081
[43] Q. Lin, J. Xu, F. Yang, J. Lin, H. Yang, Y. He. Materials **11**, *10*, 1799 (2018). https://www.mdpi.com/1996-1944/11/10/1799
[44] U.B. Gawas, V.M.S. Verenkar, S.S. Meena, P. Bhatt. J. Supercond. Nov. Magn. **30**, *11*, 3241 (2017). https://link.springer.com/article/10.1007/s10948-017-4149-7
[45] R.V. Upadhyay, R.B. Jotania, R.G. Kulkarni. Physica B **I90**, *2–3*, 183 (1993).
[46] H.M.I. Abdallah, T. Moyo, J.Z. Msomi. J. Phys.: Conf. Ser. **217**, 012141 (2010). https://iopscience.iop.org/article/10.1088/1742-6596/217/1/012141

[47] T.A. Anhøj, B. Bilenberg, B. Thomsen, C.D. Damsgaard, H.K. Rasmussen, C.S. Jacobsen, J. Mygind, S. Mørup. J. Magn. Magn. Mater. **260**, *1–2*, 115 (2003).
[48] M. Patange, S.S. Desai, S.S. Meena, S.M. Yusuf, S.E. Shirsath. RSC Adv. **5**, *111*, 91482 (2015). https://pubs.rsc.org/en/content/articlelanding/2015/ra/c5ra21522f/unauth
[49] M.I.A. Abdel Maksoud, A. El-Ghandour, G.S. El-Sayyad, R.A. Fahim, A.H. El-Hanbaly, M. Bekhit, E.K. Abdel-Khalek, H.H. El-Bahnasawy, M.A. Elkodous, A.H. Ashour, A.S. Awed. J. Inorg. Organometall. Polym. Mater. **30**, *9*, 3709 (2020). https://link.springer.com/article/10.1007/s10904-020-01523-8
[50] S.C. Bhargava, P.K. Iyengar. Physica Status Solidi (b) **53**, *1*, 359 (1972). https://doi.org/10.1002/pssb.2220530138
[51] R.S. de Biasi, L.H.G. Cardoso. Physica B **407**, *18*, 3893 (2012). http://dx.doi.org/10.1016/j.physb.2012.06.017
[52] J.Z. Msomi, W.B. Dlamini, T. Moyo, P. Ezekiel. J. Magn. Magn. Mater. **373**, 68 (2015). https://www.sciencedirect.com/science/article/abs/pii/S0304885314000559
[53] S.B. Singh, C. Srinivas, B.V. Tirupanyam, C.L. Prajapat, M.R. Singh, S.S. Meena, P. Bhatt, S.M. Yusuf, D.L. Sastry. Ceram. Int. **42**, *16*, 19179 (2016). http://dx.doi.org/10.1016/j.ceramint.2016.09.081
[54] G.A. Sawatzky, F. Van Der Woude, A.H. Morrish. Phys. Rev. **187**, *2*, 747 (1969).
[55] B.F. Bogacz, R. Gargula, P. Kurzydło, A.T. Pedziwiatr, T. Tatarchuk, N. Paliychuk. Acta Phys. Polonica. A **134**, *5*, 993 (2018).
[56] C.N. Chinnasamy, A. Narayanasamy, N. Ponpandian, K. Chattopadhyay, K. Shinoda, B. Jeyadevan, K. Tohji, K. Nakatsuka, T. Furubayashi, I. Nakatani. Phys. Rev. B **63**, *18*, 184108 (2001).
[57] G. Datt, C. Kotabage, S. Datar, A.C. Abhyankar. Phys. Chem. Chem. Phys. **20**, *41*, 26431 (2018).
[58] G.R. Patta, V. Citti Babu, V. Ravi Kumar, N. Veeraiah. J. Sol-Gel Sci. Technol. **100**, *2*, 310 (2021).
[59] T. Tatarchuk, N. Paliychuk, M. Pacia, W. Kaspera, W. Macyk, A. Kotarba, B.F. Bogacz, A.T. Pedziwiatr, I. Mironyuk, R. Gargula, P. Kurzydło, A. Shyichuk. New J. Chem. **43**, *7*, 3038 (2019).
[60] S. Morup, J.A. Dumesic, H. Topsoe. In: Applications of Mossbauer Spectroscopy / Ed. R.L. Cohen. Academic Press, N.Y. (1980). V. 2. P. 1.
[61] R.E. Vandenberghe, E. De Grave. In: Mössbauer Spectroscopy Applied to Inorganic Chemistry. Modern Inorganic Chemistry / Eds G.J. Long, F. Grandjean. Springer, Boston, MA (1989).V. 3. P. 59–182. https://doi.org/10.1007/978-1-4899-2289-2_3
[62] S. Mørup, D.E. Madsen, C. Frandsen, C.R.H. Bahl, M.F. Hansen. J. Phys.: Condens. Matter **19**, *21*, 213202 (2007).
[63] R.H. Kodama, A.E. Berkowitz, E.J. McNiff Jr, S. Foner. J. Appl. Phys. **81**, *8*, 5552 (1997). https://pubs.aip.org/aip/jap/article-abstract/81/8/5552/488705/Surface-spin-disorder-in-ferrite-nanoparticles?redirectedFrom=fulltext
[64] E. Umut, M. Coşkun, H. Güngüneş, V. Dupuis, A.S. Kamzin. J. Supercon. Nov. Magn. **34**, *3*, 913 (2021). https://doi.org/10.1007/s10948-020-05800-y
[65] Y. Yafet, C. Kittel. Phys. Rev. **87**, *2*, 290 (1952).
[66] L. Neel. J. Physique **15**, *4*, 225 (1954).
[67] A.S. Kamzin, L.A. Grigor'ev. JETP Lett. **57**, *9*, 557 (1993).
[68] A.S. Kamzin, L.A. Grigor'ev. ZETP **77**, *4*, 658 (1993).
[69] J.M.D. Coey. Phys. Rev. Lett. **27**, *17*, 1140 (1971).
[70] Mössbauer Spectroscopy Applied to Magnetism and Material Science / Eds G.J. Long, F. Grandjean. Plenum Press, N.Y. (1993). 479 p.
[71] A.S. Kamzin, V.P. Rusakov, L.A. Grigoriev. Int. Conf. USSR. Proc. Part II, 271 (1988).
[72] A.S. Kamzin, L.A. Grigor'ev. Sov. Tech. Phys. Lett. **6**, *6*, 417 (1990).
[73] A.S. Kamzin, L.A. Grigor'ev. Sov. Tech. Phys. **35**, *7*, 840 (1990).
[74] F. Schaaf, U. Gonser. Hyperfine Interact. **57**, *1–4*, 2101 (1990).
[75] U. Gonzer, P. Schaaf, F. Aubertin. Hyperfine Interact. **66**, *1–4*, 95 (1991).
[76] A.S. Kamzin, L.P. Ol'khovik, V.L. Rozenbaum. JETP **84**, *4*, 788 (1997).
[77] A.S. Kamzin. JETP **89**, *5*, 891 (1999).
[78] A.S. Kamzin, L.P. Ol'khovik, V.L. Rozenbaum. Phys. Solid State **41**, *3*, 433 (1999).
[79] A.S. Kamzin, V.L. Rozenbaum, L.P. Ol'khovik. JETP Lett. **67**, *10*, 843 (1998).
[80] A.S. Kamzin, L.P. Ol'khovik. Phys. Solid State **41**, *10*, 1658 (1999).
[81] A.S. Kamzin, I.M. Obaidat, A.A. Valiullin, V.G. Semenov, I.A. Al-Omari. Phys. Solid State **62**, *10*, 1933 (2020). DOI: https://link. springer.com/article/10.1134/S1063783420100157
[82] M.E. Matsnev, V.S. Rusakov. AIP Conf. Proc. **1489**, *1*, 178 (2012).
[83] G.N. Konygin, O.M. Nemtsova, V.E. Porsev. Zhurn. priklad. spektroskopii **86**, *3*, 374 (2019). (in Russian).

Translated by A.Akhtyamov